MISR aerosol optical depth retrievals over southern Africa during the SAFARI-2000 dry season campaign

D. J. Diner, W. A. Abdou, C. J. Bruegge, J. E. Conel, K. A. Crean,
B. J. Gaitley, M. C. Helmlinger, R. A. Kahn, J. V. Martonchik, S. H. Pilorz

Jet Propulsion Laboratory, California Institute of Technology, Pasadena, California

B. N. Holben

Goddard Space Flight Center, Greenbelt, Maryland

Abstract. This paper presents, for the first time, retrievals of aerosol optical depths from Multi-angle Imaging Spectro-Radiometer (MISR) observations over land. Application of the MISR operational algorithm to data taken over southern Africa during the SAFARI-2000 dry season campaign yields results that compare favorably with coincident surface-based measurements taken by the AERONET radiometer network.

Introduction

MISR [*Diner et al.*, 1998] was launched into polar Earth orbit aboard the Terra spacecraft in Dec. 1999. Its objectives include the global study of aerosol sources, sinks, and shortwave radiative properties. Key aerosol source regions occur on land, but the brightness and heterogeneity of the surface presents a challenge to space-based aerosol retrievals.

During Aug.-Sept. 2000, the MISR team participated in the dry season campaign of the Southern Africa Regional Science Initiative (SAFARI-2000), aimed at studying transport and deposition of regional aerosols. Grassland fires and industrial pollution generated a range of aerosol conditions. Concurrently, the Aerosol Robotic Network (AERONET), an automated array of Sun-sky scanning CIMEL radiometers [*Holben et al.*, 1998], provided surface-based measurements from which spectral aerosol optical depth (AOD) and particle properties were derived [*Dubovik and King*, 2000]. This paper compares MISR AOD retrievals over land during SAFARI-2000 with coincident AERONET results.

MISR aerosol retrievals over land

MISR images the Earth at nine discrete view angles, from nadir up to 70.5° fore and aft of the local vertical. Multispectral (446, 558, 672, and 866 nm) imagery is obtained at each angle. MISR globally provides 275-m sampling in all bands of the nadir camera and the red band of each of the off-nadir cameras, and 1.1 km for the remaining channels. It takes 7 minutes for all nine cameras to image a given location. Terra is in a sun-synchronous orbit, and crosses the equator at approximately 10:45 AM (local time) on the dayside.

Spaceborne aerosol retrievals over land require disentangling the surface- and atmosphere-leaving signals. Some methods rely upon empirical spectral relationships over dense vegetation [*Kaufman et al.*, 1997] or exploit the low magnitude and variability of ultraviolet surface albedo [*Torres et al.*, 1998]. An approach devised for the Along-Track Scanning Radiometer-2 [*North et al.*, 1999] assumes spectral invariance of the surface signal between the sensor's two angles.

The operational MISR aerosol retrieval "beta" software is in the early stages of verification and validation. Radiometrically calibrated, geo-located radiances at 1.1-km resolution are used to derive empirical orthogonal functions (EOF's) representing the angular shape of the surface signal within 17.6×17.6 km^2 regions. This procedure [*Martonchik et al.*, 1998] requires scene spatial contrasts but does not invoke assumptions about the absolute surface reflectance or its spectral characteristics. To constrain the retrievals, the algorithm establishes candidate aerosol models, each with specified proportions of three component particle types having prescribed microphysical properties. Path radiances are calculated using a modified linear mixing approach [*Abdou et al.*, 1997]. Least-squares optimization simultaneously provides the coefficients of the dominant surface EOF's and the 558-nm AOD associated with modeled atmospheric path radiances, and successful retrievals require a specified goodness-of-fit to the observations. Updates to the algorithm are documented on-line *(http://eospso.gsfc.nasa.gov/atbd/misrtables.html)*.

Five aerosol models, chosen to provide a climatologically reasonable range of optical properties, are used globally over land. The characteristics of the component particles making up these models were established prior to launch from a review of published aerosol climatologies [*d'Almeida et al.*, 1991; *Krekov*, 1993; *Shettle and Fenn*, 1979; *World Climate Programme*, 1984]. The sulfate/nitrate component particles are spherical, and log-normally distributed with mode ra-

Table 1. Characteristics of the five aerosol models.

	1	2	3	4	5
Sulfate/nitrate fractional AOD	0.95	0.90	0.85	0.80	0.75
Mineral dust fractional AOD	0.00	0.00	0.00	0.00	0.25
Black carbon fractional AOD	0.05	0.10	0.15	0.20	0.00
ω_{558}	0.960	0.921	0.881	0.842	0.984
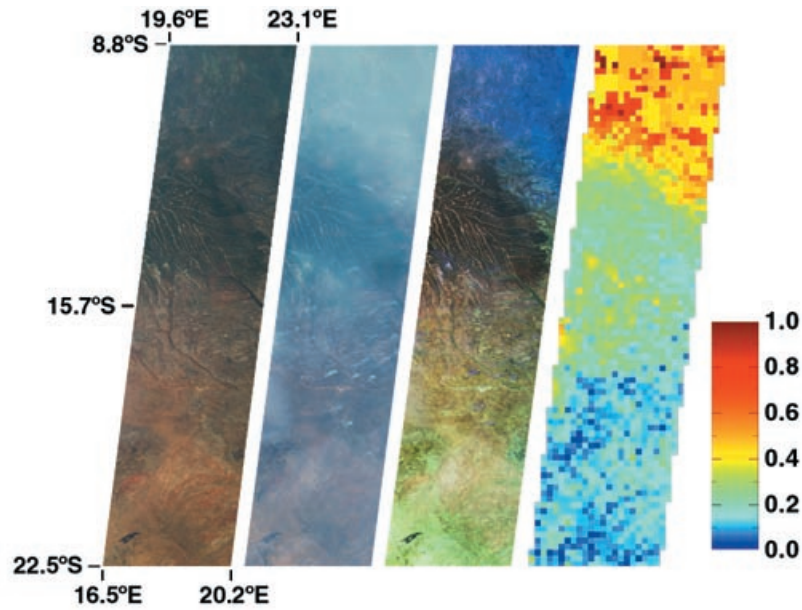
Figure 1. MISR data over eastern Angola and northeastern Namibia acquired on 30 August 2000 (Terra orbit 3728). Images from left to right are: red, green, blue (RGB) composite of radiometrically calibrated, geo-located data from the nadir camera; RGB composite from the backward-viewing 70.5° camera; multi-angle composite of imagery from the red band of the nadir camera (displayed as red), the forward 70.5° camera (displayed as green), and the backward 70.5° camera (displayed as blue). In the latter, color is a proxy for angular, rather than spectral, scene content; blue-purple hues signify enhanced optical depth. RMOD retrievals are given on the right; the pixellation shows individual 17.6×17.6 km² regions. Swaths are roughly 380 km wide.

dius (r_m) of 0.08 μm, characteristic width (σ) of 1.88, and refractive index at 558 nm (n_{558}) of $1.46 - 0.0i$ at 0% relative humidity. They are hydrated to a relative humidity of 70%, following [*Hanel*, 1976]. The mineral dust component is a monodisperse distribution of randomly oriented prolate and oblate spheroids having $r_m = 0.47$ μm and n_{558} $= 1.53 - 0.0055i$ [*Mishchenko et al.*, 1997]. The black carbon particles are spherical and log-normally distributed with $r_m = 0.012$ μm, $\sigma = 2.00$, and $n_{558} = 1.75 - 0.44i$. The fractional 558-nm AOD's of the component particles and the effective single-scattering albedo, ω_{558}, for the models are summarized in Table 1.
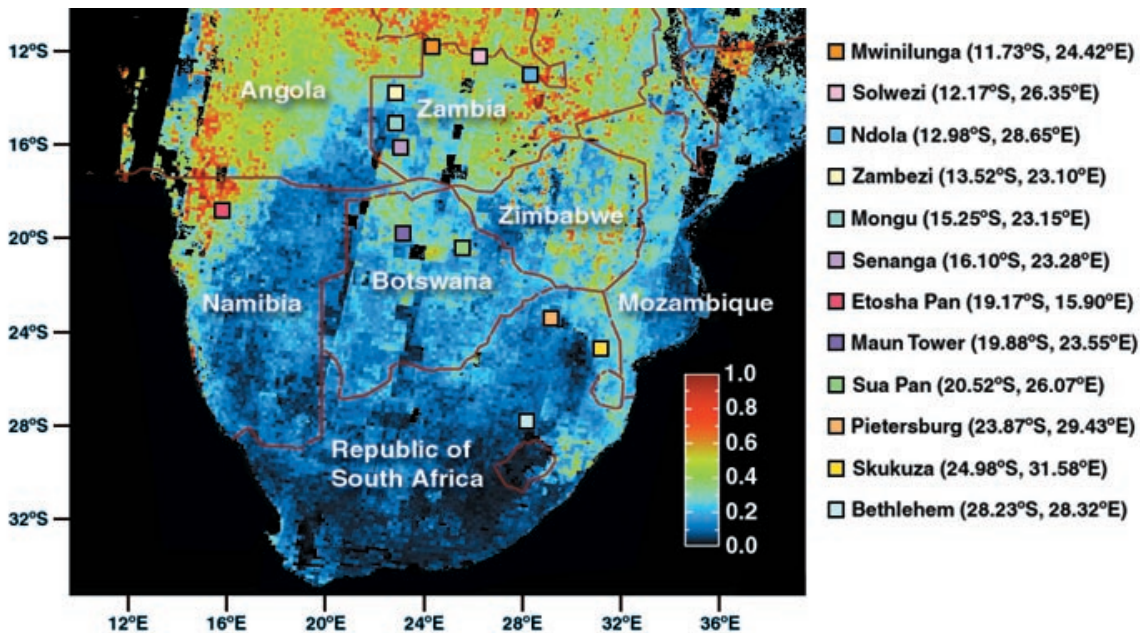
Figure 2. Mosaic of 558-nm RMOD over southern Africa, from 27 orbits of MISR data acquired 14 August-29 September 2000. The data cover World Reference System-2 paths 165-183, and are reprojected to a 3-arcmin equiangular grid. Missing land data are shown as black. Locations of the 12 AERONET sites with coincident MISR retrievals are marked. The lowest optical depths occur over the Drakensberg Mountains, which run from the south through Lesotho (south of Bethlehem) to the northeast between Skukuza and Pietersburg.

Results

The first-generation MISR algorithm over land is aimed primarily at retrieving AOD, and refinements to improve discrimination by particle type are underway. AOD at 558 nm, averaged over all successful models within a 17.6×17.6 km^2 region, is reported as the "regional mean optical depth" (RMOD) in the MISR Aerosol product. Figure 1 is an example of how MISR facilitates aerosol retrievals over land. Note how the steep view angle accentuates smoke plumes and haze. The rightmost panel presents retrieved RMOD.

Figure 2 is a mosaic of RMOD spanning 14 Aug.-29 Sept. 2000, derived from 27 orbits for which data were available from the NASA Langley Atmospheric Sciences Data Center (ASDC) and processed into aerosol and cloud products. A persistent pattern is observed in spite of the 6-week time interval. In the northern part of this map, where vegetation is more abundant and grassland fires more prevalent, MISR observes the highest RMOD. The lowest values are found over the Drakensberg Mountains in eastern South Africa. Although the data were acquired at the local time of the Terra overpass, AOD from late morning seems to be a good predictor of the daily mean [*Kaufman et al.*, 2000].

Several approaches were used to screen the MISR retrievals for clouds, all of which exploit the geometric parallax associated with viewing clouds from different angles. First, within a 17.6×17.6 km^2 region, only those 1.1-km-resolution radiances that vary smoothly with angle are used in the aerosol retrievals. Second, using 275-m resolution red band data, 1.1-km areas were required to exhibit a positive spatial correlation from one angle to another. A third filter, based upon the stereoscopic cloud mask generated as part of the MISR Cloud product suite, was also applied. It uses automated pattern recognition to establish the parallax field from which the spatially-varying height of the reflecting surface is derived at 1.1-km resolution. A "Clear" designation requires this altitude to be within a few hundred meters of the terrain. Multiple cameras are used to simultaneously establish cloud displacements due to parallax as well as wind-driven motion over the 7-minute observing interval [*Horvath and Davies*, 2001].

Figure 3 compares MISR retrievals with AERONET data interpolated to 558 nm. Each AERONET AOD is an average of three observations made 30 seconds apart. To assess spatial and temporal variability, we computed the standard deviation of AOD within ± 30 minutes of the Terra overpass. A quality assessment (QA) status of "excellent" is assigned if the standard deviation is < 0.01, "good" if < 0.02, "fair" if < 0.04, and "questionable" if > 0.04 or if the data were acquired more than 25 minutes from the overpass time. Four points are labelled "no QA" due to lack of post-field calibration; however, their standard deviations are low indicating good temporal stability.

To quantify the uncertainties in the MISR retrievals, RMOD data from a 3×3 set of 17.6×17.6 km^2 regions centered on each AERONET site were averaged, and the standard deviation used as a measure of uncertainty. It has three principal contributors: (a) variability due to non-unique fits by multiple models, (b) algorithmic noise due to imperfect separation of the atmospheric and surface signals, and (c) natural spatial AOD variability. Figure 1 suggests that, away from the source regions, AOD varies on spatial scales large compared to the resolution of the MISR retrievals. Assuming (c) is small, the contributions of (a) and (b) to the

Table 2. Site locations, dates, times of AERONET and MISR observations, and their time differences.

Site	Date	t_{AERO} (GMT)	t_{MISR} (GMT)	Δt (mm:ss)
Mwinilunga	8/25	8:54:48	8:55:34	0:46
	9/10	8:49:50	8:55:35	5:45
Solwezi	8/25	9:02:11	8:55:34	6:37
	9/3	8:44:29	8:49:34	5:05
	9/10	8:57:09	8:55:35	1:34
Ndola	9/5	9:04:20	8:37:27	26:53
Zambezi	8/16	9:02:19	9:02:03	0:16
	8/23	8:37:39	9:08:17	30:38
Mongu	8/16	9:01:32	9:02:30	0:58
	9/26	8:04:32	8:56:05	51:33
Senanga	8/16	9:01:26	9:02:43	1:17
	9/26	8:48:38	8:56:18	7:40
Etosha Pan	8/28	9:28:12	9:28:32	0:20
	9/29	9:32:04	9:27:52	4:12
Maun Tower	9/26	9:02:42	8:57:17	5:25
Sua Pan	9/3	8:45:37	8:51:46	6:09
Pietersburg	9/7	8:30:53	8:28:05	2:49
Skukuza	8/31	8:28:05	8:22:10	5:55
	9/7	8:37:50	8:28:14	9:36
	9/9	8:22:11	8:16:03	6:08
Bethlehem	8/29	8:39:49	8:35:23	4:26
	9/7	8:36:00	8:29:18	6:42
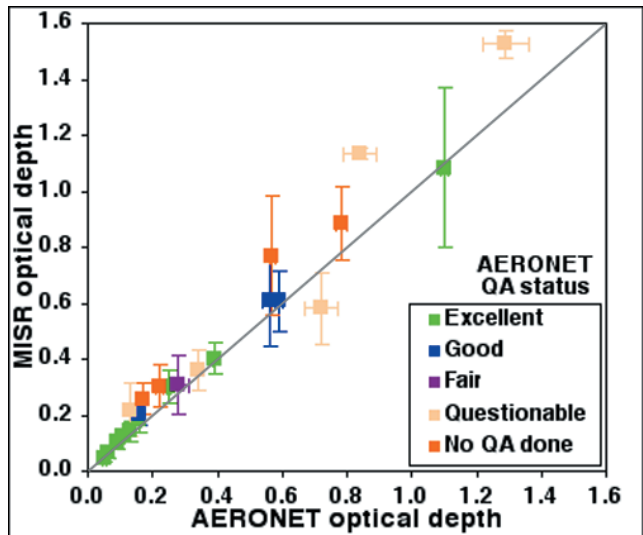
Figure 3. Comparison between 558-nm 3×3 averages of RMOD retrieved from MISR data, and coincident AOD derived from AERONET. The 1:1 line is shown. The 22 data points in this plot are all over land, and correspond to 12 unique site locations in southern Africa. Points are color coded by their AERONET QA status.

variances are typically comparable. Results from all available coincident MISR/AERONET data are included in Figure 3, provided that there was at least one successful RMOD retrieval within the 3×3 set of regions, and the stereo cloud mask indicated "Clear" at the site location. Table 2 provides a detailed site summary.

Figure 3 shows a good linear correlation between MISR and AERONET retrievals. Fitting all the data yields a slope of 1.10 and intercept of 0.02. Thin cirrus clouds, which particularly affect the oblique MISR images but which may not always be present in the AERONET line of sight, could account for the small bias. Since cirrus can cause temporal variability in the CIMEL AOD's, we excluded the "questionable" AERONET points from the regression. When this is done, the slope is 1.03 and the intercept is 0.03. Implementation of a band-difference angular signature algorithm [*Di Girolamo and Davies*, 1994] to improve the screening of cirrus clouds in MISR data is planned.

Additional next steps include observationally-driven updates to the particle models and algorithm improvements to discriminate particle types. Analysis of co-located AERONET and MISR data on a world-wide basis, along with results from campaigns such as SAFARI [e.g., *Hobbs*, 2001], will help refine our aerosol retrieval methodologies. MISR data are publicly available through the ASDC *(http://eosweb .larc.nasa.gov)*.

References

Abdou, W.A., J.V. Martonchik, R.A. Kahn, R.A. West, and D.J. Diner, A modified linear mixing method for calculating atmospheric path radiances of aerosol mixtures, *J. Geophys. Res., 102,* 16883-16888, 1997.

d'Almeida, G.A., P. Koepke, and E.P. Shettle, *Atmospheric aerosols: Global climatology and radiative characteristics,* Deepak Publishing, Hampton, VA, 1991.

Di Girolamo, L. and R. Davies, A band-differenced angular signature technique for cirrus cloud detection, *IEEE Trans. Geosci. Rem. Sens., 32,* 890-896, 1994.

Diner, D., J. Beckert, T. Reilly, C. Bruegge, J. Conel, R. Kahn, J. Martonchik, T. Ackerman, R. Davies, S. Gerstl, H. Gordon, J-P. Muller, R. Myneni, P. Sellers, B. Pinty, and M. Verstraete, Multi-angle Imaging SpectroRadiometer (MISR) instrument description and experiment overview, *IEEE Trans. Geosci. Rem. Sens., 36,* 1072-1087, 1998.

Dubovik, O., and M.D. King, A flexible inversion algorithm for retrieval of aerosol optical properties from Sun and sky radiance measurements, *J. Geophys. Res., 105,* 20673-20696, 2000.

Hanel, G, The properties of atmospheric aerosol particles as functions of relative humidity at thermodynamic equilibrium with the surrounding moist air, *Adv. Geophys., 19,* 73, 1976.

Hobbs, P.V., *Summary of flights and types of data collected aboard the Univ.of Washington's Convair-580 research aircraft in the SAFARI-2000 field study in southern Africa from 10 August through 18 September 2000,* available from http://cargsun2.atmos.washington.edu/sys/research/safari /SAFARI-MASTER-02.01.pdf, University of Washington, 2001.

Holben, B.N., T.F. Eck, I. Slutsker, D. Tanre, J.P. Buis, A. Setzer, E. Vermote, J.A. Reagan, Y.J Kaufman, T. Nakajima, F. Lavenu, I. Jankowiak, and A. Smirnov, AERONET–a federated instrument network and data archive for aerosol characterization, *Remote Sens. Environ., 66,* 1-16, 1998.

Horvath, A. and R. Davies, Feasibility and error analysis of cloud motion wind extraction from near simultaneous multiangle MISR measurements, *J. Atmos. Oceanic Tech., 18,* 591-608, 2001.

Kaufman, Y.J., D. Tanre, L.A. Remer, E.F. Vermote, A. Chu, and B.N. Holben, Operational remote sensing of tropospheric aerosol over land from EOS moderate resolution imaging spectroradiometer, *J. Geophys. Res., 102,* 17051-17067, 1997.

Kaufman, Y.J., B.N. Holben, D. Tanre, I. Slutsker, A. Smirnov, and T.F. Eck, Will aerosol measurements from Terra and Aqua polar orbiting satellites represent the daily aerosol abundance and properties? *Geophys. Res. Lett., 27,* 3861-3864, 2000.

Krekov, G.M, Models of atmospheric aerosols, in *Aerosol Effects on Climate,* edited by S.G. Jennings, Univ. of Arizona Press, Tucson, AZ, 1993.

Martonchik, J.V., D.J. Diner, R.A. Kahn, T.P. Ackerman, M.M. Verstraete, B. Pinty, and H.R. Gordon, Techniques for the retrieval of aerosol properties over land and ocean using multiangle imaging, *IEEE Trans. Geosci. Rem. Sens., 36,* 1212-1227, 1998.

Mishchenko, M.I., L. Travis, R. Kahn, and R. West, Modeling phase functions for dust-like tropospheric aerosols using a shape mixture of randomly oriented polydisperse spheroids, *J. Geophys. Res., 102,* 16831-16847, 1997.

North, P.R.J., S.A. Briggs, S.E. Plummer, and J.J. Settle, Retrieval of land surface bidirectional reflectance and aerosol opacity from ATSR-2 multi-angle imagery, *IEEE Trans. Geosci. Rem. Sens., 37,* 526-537, 1999.

Shettle, E.P. and R.W. Fenn, *Models for the aerosols of the lower atmosphere and the effects of humidity variations on their optical properties, AFGL-TR-79-0214,* Air Force Geophys. Lab., Hanscom AFB, MA, 1979.

Torres, O., P.K. Bhartia, J.R. Herman, Z. Ahmad, and J. Gleason, Derivation of aerosol properties from satellite measurements of backscattered ultraviolet radiation: Theoretical basis, *J. Geophys. Res., 103,* 17099-17110, 1998.

World Climate Programme, *A preliminary cloudless standard atmosphere for radiation computation, WCP-112,* IAMAP, Boulder, CO, 1984.

D. J. Diner, W. A. Abdou, C. J. Bruegge, J. E. Conel, K. A. Crean, B. J. Gaitley, M. C. Helmlinger, R. A. Kahn, J. V. Martonchik, S. H. Pilorz, Jet Propulsion Laboratory, California Institute of Technology, Mail stop 169-237, 4800 Oak Grove Drive, Pasadena, CA 91109

B. N. Holben, NASA Goddard Space Flight Center, Code 923, Greenbelt, MD 20771